Dalton Transactions

ROYAL SOCIETY OF CHEMISTRY

PAPER

View Article Online
View Journal | View Issue

Cite this: *Dalton Trans.*, 2022, **51**, 15965

Uranium oxide hydrate frameworks with Er(III) or Y(III) ions: revealing structural insights leading to the low symmetry†

Timothy A. Ablott, Kimbal T. Lu, Robert D. Aughterson and Yingjie Zhang *

Received 25th August 2022,
Accepted 28th September 2022

DOI: 10.1039/d2dt02763a

rsc.li/dalton

Two new mixed-valence uranium oxide hydrate frameworks (UOFs), incorporating either Er^{3+} or Y^{3+} ions, were successfully synthesised under hydrothermal conditions and characterised with single-crystal X-ray diffraction and a variety of other structural and spectroscopic techniques. Both frameworks are isostructural and crystallise in the triclinic $P\bar{1}$ space group, consisting of β-U_3O_8 type layers pillared by additional uranyl centres, with the Er^{3+}/Y^{3+} ions lying in the channels of the framework. SEM-EDS analysis found that both materials existed in plate-like morphologies, with a U:Er/Y ratio of 5.5. Bond valence sum analysis revealed the possible existence of pentavalent uranium centres, which was confirmed with diffuse reflectance spectroscopy. Being the first reported UOFs in this space group, this work highlights the complex and flexible nature of these materials, and the broader uranium oxide hydrate systems which exist in the surrounds of spent nuclear fuel disposal in the underground repository.

1. Introduction

The study of uranium oxide synthetic compounds has seen significant interest and substantial exploration due to their close relationship with the uranium oxide systems used as nuclear fuel in nuclear reactors around the world.[1,2] With a push towards cleaner energy production to combat climate change, nuclear energy has again become a focus for many countries.[1,2] One issue clearly identified with these fuel systems is the need for the safe management and disposal of the spent nuclear fuel (SNF) once removed from the nuclear reactor, in order to isolate these highly radioactive materials from the general public.[3,4] With a variety of options available, changing from country to country, one of the most widely accepted approaches is the disposal of SNF in stable underground geological repositories, wherein the SNF is essentially safely isolated from the outside world.[2] To ensure this isolated SNF, most commonly present as uranium oxide (UO_2), is safe to store within these repositories for the long-term, studies into the behavior of these materials in these geological environments are critical.

Both natural and synthetic uranium oxide compounds have proven extremely useful in replicating the conditions that these SNFs are exposed to in the repository environment. The study of these uranium oxide compounds has been driven by the knowledge of the natural weathering of uraninite (UO_{2+x}).[5,6] When exposed to oxidative conditions uraninite is known to undergo oxidation from U^{4+} to U^{6+}, often existing in the form of uranyl [$(UO_2)^{2+}$] cations which further react with electron donors in the surrounding environment, forming a plethora of uranyl oxide compounds.[7,8] These uranyl moieties typically contain two strongly bound oxygen atoms in the axial positions, with the equatorial positions regularly binding additional O^{2-} or OH^- ions, giving rise to typical coordination geometries of tetragonal, pentagonal, or hexagonal bipyramidal polyhedra.[9,10] Extension of these polyhedra *via* corner- or edge-sharing results in the formation of layered (sheet) structures, which are commonly bridged by interlayer cations. Logically, given their compositions, these materials have been assigned the name uranium oxide hydrates (UOH).[11,12] The study of uranium-containing minerals has identified several dozen UOH-based minerals,[1,11] and with this knowledge more than a dozen synthetic UOH materials have since been reported.[13–18] The distinctive features in these materials are the differing secondary metal ions which make up the interlayer cation layer, and the O : OH ratios of the uranyl oxide hydroxide sheets.

A subset of UOH materials are those labelled uranium oxide frameworks, or UOFs. They differ from UOHs in that they form a framework-type structure, with uranyl oxide moieties linking two layered sheets, with the secondary cations lying within the channels formed by these linkers. A small but

Australian Nuclear Science and Technology Organisation, Locked Bag 2001, Kirrawee DC, NSW 2232, Australia. E-mail: yzx@ansto.gov.au

†Electronic supplementary information (ESI) available: SEM-EDS. CCDC 2192943 (**UOF-Y**) and 2192944 (**UOF-Er**). For ESI and crystallographic data in CIF or other electronic format see DOI: **https://doi.org/10.1039/d2dt02763a**

wide variety of secondary cations have been successfully incorporated into these UOF structures, including Cs^{+}, Sr^{2+}, Pb^{2+}, Sm^{3+}, Eu^{3+}, Gd^{3+} and U^{4+}.[19–24] Given the evident diversity of what can be stabilised within the channels of these materials, further study is therefore needed in this field in order to truly capture the possible chemistry which can occur in the surrounds of the SNF disposed within a deep geological repository.

With lanthanides often found alongside uranium in the environment, as well as being present in SNF as fission products, they are therefore expected to be heavily involved in the modification of both natural UOH minerals and synthetic UOH compounds. In addition, they can also be applied as surrogates for minor actinides (*i.e.* Am^{3+} and Cm^{3+}) which would also be present in the SNF environment,[25,26] which makes Ln^{3+} species an ideal target of study for synthetic UOHs. Up to this point, no natural UOH minerals containing lanthanides have been identified, thus this area has been driven by synthetic UOH research. Early research into these synthetic compounds discovered both the uranium precursor as well as starting pH, which controls uranium hydrolysis, were crucial in their successful synthesis. Research using a schoepite precursor first led to the successful incorporation of a variety of Ln ions (Ln = Tb, Dy, Ho and Yb) between α-U_3O_8 uranyl oxide layers, with a U:Ln ratio of 2.[27] Interestingly, in 2020 Lu *et al.* were able to synthesise a second UOH-Tb material with a U:Tb ratio of 6 and a different uranyl oxide hydroxide layer topology, now resembling a β-U_3O_8 uranyl oxide layer.[28] This highlighted the potential for the interlayer cations to directly affect the chemistry of the uranyl oxide layers within these materials. Other UOH-Ln compounds have also been reported sans crystal structures, clearly demonstrating the challenge that exists in obtaining single crystals of UOH-Ln which are of high enough purity for single crystal analysis. These UOH-Ln compounds are listed in Table 1.

Intriguingly, as evidenced by Table 1, only Sm, Eu and Gd have been found to form the UOF sub-structure, with the Ln^{3+} ions found within the 3D channels of the framework.[21,22] However, this work has also found that the pH of the synthesis is highly influential on the formation of either a UOF or UOH structure. For UOH/F-Sm, a synthesis pH < 4 gave rise to a UOF structure, whereas increasing the pH to 4–5 resulted in a layered UOH material in its place.[21] This further highlights the complex synthetic chemistry of these materials, driving the need for further research. It has also been hypothesised as to whether the preferential formation of a Ln^{3+} containing UOF-type structure over a UOH-layered material is moderated by the ionic radius of the selected cation.[12] Given, of the lanthanide structures reported, the three which all have very similar ionic radii are the only ones to form a framework structure, this suggestion has merit. Thus, erbium, having a smaller ionic radius to those of Sm, Eu and Gd, is a prime candidate to probe such a hypothesis. Only one synthesis of a UOH-Er material has been reported, however no single-crystal analysis was done on the material which prevented any structural insights from being explored.[30] Yttrium was a second candidate that was identified for this study, with no previously reported structures containing Y having been found. Being chemically similar to Ln^{3+} ions and having an ionic radius close to that of erbium, it was selected as a possible UOH/F-Ln surrogate which could further aid in the understanding of the chemistry driving the formation of these materials. Herein, we report the hydrothermal synthesis of two novel synthetic UOF compounds, **UOF-Er** and **UOF-Y**, and their structural and spectroscopic analyses. The crystals isolated from the hydrothermal reaction of uranyl nitrate with either Er^{3+} or Y^{3+} ions were revealed to have an as of yet unseen 3D framework-type structure *via* synchrotron single crystal X-ray diffraction analysis, with the crystals subsequently explored using scanning and transmission electron microscopy alongside Raman and diffuse reflectance spectroscopy.

2. Experimental

2.1. Syntheses of materials

Uranyl nitrate hexahydrate with natural uranium was used in the synthesis of the materials. Compounds with uranium are radioactive and should be handled in the regulated laboratory. All other chemicals in A.R. grade were from Sigma-Aldrich (Merck).

2.1.1 $Er_2(H_2O)_8[(UO_2)_{10}UO_{14}(OH)_3]$ (UOF-Er). Erbium nitrate pentahydrate, $Er(NO_3)_3{\cdot}5H_2O$, (0.0731 g, 0.165 mmol) and uranyl nitrate hexahydrate (0.0828 g, 0.165 mmol) were dissolved in 5 mL deionized (DI) water, followed by the addition of 1 M NaOH (2 mL). The solution of pH 6.18, with equal concentration of Er^{3+} and $(UO_2)^{2+}$ (0.0236 M L^{-1}), was transferred into a 30 mL Teflon vessel, sealed in a steel autoclave and heated in an oven at 200 °C for 48 hours. Small orange crystals of compound **UOF-Er** were obtained after

Table 1 A summary of synthetic UOH materials containing Ln^{3+} species[21,22,27–30]

UOH-Ln^{3+}	U/Ln ratio	Single crystal structure	Other characterization
UOH-Sm	1	No	XRD, SEM-EDS, TG
UOH-La/Pr/Nd/Tb/Dy/Ho/Yb	2	Yes	XRD, SEM-EDS, TEM, Raman, UV-vis, TG
UOH-Dy/Ho/Er/Tm/Tb/Yb/Lu	2	No	XRD, IR, TG
UOH-La/Ce/Pr/Nd/Sm	3	No	XRD, IR, TG
UOH-Sm	4	No	XRD, SEM-EDS
UOF-Sm/Eu/Gd	5.5	Yes	XRD, SEM-EDS, TEM, Raman, UV-vis-NIR, TG
UOH-Tb	6	Yes	—
UOH-Nd/Sm/Eu/Gd/Tb/Dy	6	No	XRD, IR, TG

cooling to room temperature at 4 °C h^{-1} with the final solution pH 5.16. The crystals of compound **UOF-Er** were washed with DI water and dried at 50 °C overnight (0.0351 g isolated, 62% yield based on uranium). The synthesis for compound **UOF-Er** was repeated, with similar SEM-EDS results and yields obtained.

2.1.2 $Y_2(H_2O)_8[(UO_2)_{10}UO_{14}(OH)_3]$ (UOF-Y). Yttrium nitrate hexahydrate, $Y(NO_3)_3{\cdot}5H_2O$, (0.0582 g, 0.151 mmol) and uranyl nitrate hexahydrate (0.0838 g, 0.167 mmol) were dissolved in 5 mL DI water, followed by the addition of 1 M NaOH (1 mL). The solution of pH 5.88, with concentrations of Y^{3+} (0.0252 M L^{-1}) and $(UO_2)^{2+}$ (0.0278 M L^{-1}), was transferred into a 30 mL Teflon vessel, sealed in a steel autoclave and heated in an oven at 240 °C for 72 hours. Small orange crystals of compound **UOF-Y** were obtained after cooling to room temperature at 2.5 °C h^{-1} with the final solution pH 4.23. The crystals of compound **UOF-Y** were washed with DI water and dried at 50 °C overnight (0.0262 g isolated, 49% yield based on uranium).

2.2. Characterizations

2.2.1. Synchrotron single crystal X-ray diffraction. The single crystal data for compounds **UOF-Y** (CSD-2192943†) and **UOF-Er** (CSD-2192944†) were collected at 100(2) K on the MX2 beamline[31] at the Australian Synchrotron employing silicon double crystal monochromated synchrotron radiation (λ = 0.71089–0.71093 Å). Data integration and reduction were undertaken with XDS.[32] Absorption corrections were applied to the data using SADABS.[33] The structures were solved by direct methods[34] and refined with SHELXL-2014[35] using the Olex^2 graphical user interface.[36] All atoms with ≥0.5 occupancies were located on the electron density maps and refined anisotropically. Hydrogen atoms on hydroxyl groups and water molecules were unable to be located and they were omitted in the structure refinements. Both compounds contain U as a strong X-ray absorber. In addition, the one-circle goniometer setup on the MX2 beamline provided less redundant data for absorption corrections. As such there were some Q-peaks around U atoms due to the ineffective absorption corrections.

2.2.2. Scanning electron microscopy (SEM) and transmission electron microscopy (TEM). The crystal morphologies and elemental compositions were analysed using SEM coupled with energy dispersive spectrometry (EDS). Samples were carbon coated and examined in a Zeiss Ultra Plus scanning electron microscope (Carl Zeiss NTS GmbH, Oberkochen, Germany) operating at 15 kV equipped with an Oxford Instruments X-Max 80 mm^2 SDD X-ray microanalysis system. EDS point analyses were carried out on relatively flat crystal surfaces with Cu standard for calibration. Small amounts of finely ground, *via* mortar and pestle, crystal fragments were suspended in ethanol and then dispersed on a TEM holey-carbon film with copper support. The specimen was then characterised using a JEOL 2200FS (JEOL Ltd, Japan) TEM operated at 200 kV, fitted with an Oxford X-Max silicon drift detector for energy dispersive X-ray analysis (EDS). EDS data were analysed using the Oxford INCA v.4.15 microanalysis software.

2.2.3. Crystal topologies. The crystal topology analyses were performed using topcryst.com.[37] The RCSR three-letter codes[38] were used to designate the network topologies. Those nets, that are absent in the RCSR, are designated with the TOPOS NDn nomenclature,[39] where *N* is a sequence of coordination numbers of all non-equivalent nodes of the net, D is periodicity of the net (D = M, C, L, T for 0-, 1-, 2-, 3-periodic nets), and n is the ordinal number of the net in the set of all non-isomorphic nets with the given ND sequence. To calculate the underlying nets, we used algorithms,[39] the application of which for specific structures is discussed in the article.[40] The TTD collection[41] was used to determine the topological type of the crystal structure.

2.2.4. Raman spectroscopy. Raman spectra were collected on a Renishaw inVia spectrometer equipped with a 785 nm excitation Ar laser in the range of 2000–100 cm^{-1} with a spectral resolution of ~1.7 cm^{-1}.

2.2.5. Diffuse reflectance spectroscopy (DRS). Absorption spectra in both the UV-visible and near-infrared (NIR) regions were recorded on an Agilent Cary 5000 spectrophotometer equipped with a Labsphere Biconical Accessory and referenced to a Labsphere certified standard.

3. Results and discussion

3.1. Material synthesis, microstructure and U to Er/Y ratios

Both **UOF-Er** and **UOF-Y** were successfully synthesised using uranyl nitrate as uranium precursor, with the solution pH directly controlled using NaOH. The formation of **UOF-Er** was achieved by dissolving equimolar amounts of $UO_2(NO_3)_2{\cdot}6H_2O$ and $Er(NO_3)_3{\cdot}5H_2O$ in H_2O and adjusting the starting pH to 6.18, with the solution then subsequently heated at 200 °C for 48 hours. Similarly, **UOF-Y** was synthesised using an almost identical procedure, with equimolar $UO_2(NO_3)_2{\cdot}6H_2O$ and $Y(NO_3)_3{\cdot}6H_2O$ first dissolved in water, with the pH adjusted to 5.88. The solution was then heated at 240 °C for 72 hours.

SEM analysis of **UOF-Er** revealed the presence of two distinct crystal morphologies. The major phase exists as large blocks/plates (Fig. 1a, left), with the minor phase consisting of thin plates, a very common crystal morphology for both synthetic UOH compounds[20,27,28] and UOH minerals.[42] SEM-EDS analysis of the major phase confirmed the presence of only U, Er and O in the material, with a U:Er ratio of ~5.7 (Fig. 1a, right, Fig. S1 and Table S1, ESI†). The minor phase also contained only U, Er and O in the material, with a U:Er ratio of ~2.5 (Fig. S2 and Table S1, ESI†), again consistent with other synthetic UOH materials.[20,27,28] The EDS results are consistent with the major phase existing as a UOF with the minor phase that of a layered UOH material. Given these systems are known to be complex and can readily be influenced by reaction conditions (temperature, duration and solution pH), these findings are not entirely surprising. As such, the synthetic conditions reported for **UOF-Er** appear to allow for several phases to co-exist, with **UOF-Er** existing as the major phase.

UOF-Y was consistent with the findings of **UOF-Er**, with two phases immediately apparent upon examination with SEM. The major phase is present in the similar block/plate-like mor-

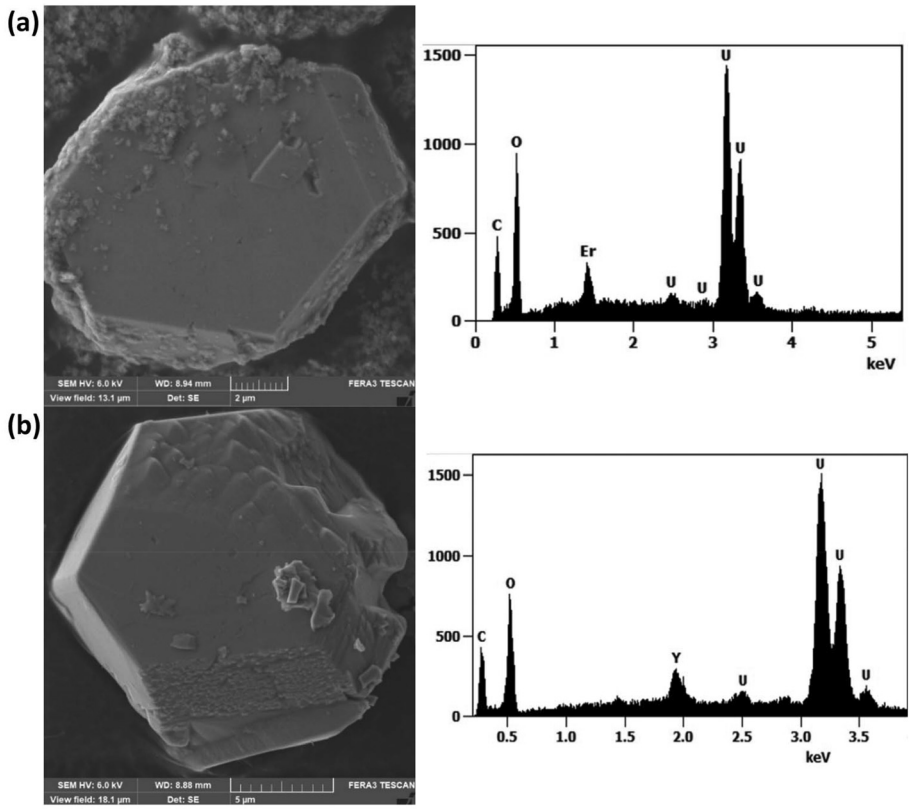

Fig. 1 SEM analysis of (a) **UOF-Er** and (b) **UOF-Y**: secondary SEM images of the crystals on the left and their corresponding EDS spectra on the right confirming the presence of both U and the Er/Y in a ~5.5 : 1 atomic ratio.

phology (Fig. 1b, left), with SEM-EDS analysis indicating a U:Y ratio of ~5.8 (Fig. 1b, Fig. S3 and Table S1, ESI†), also confirming the presence of only U, Y and O in the crystal. The minor phase gave a U:Y ratio of ~3 (Table S1, ESI†) and appeared in the similar small plates, likely to exist as a layered UOH structure. Given the complexity of separating these two phases, and with the minor phase seemingly existing as a UOH structure, further characterization of this phase was not carried out.

3.2. Crystal structures and discussion

The crystal data and structural refinement details for compounds **UOF-Er** and **UOF-Y** are summarised in Table 2, with selected bond lengths (Å) and angles (°) in Table S2, ESI.† The calculated bond valence sums (BVSs)[9] are presented in Tables S3 and S4, ESI,† with the parameters for U^{6+} taken from the literature.[9,43]

Both compounds **UOF-Er** and **UOF-Y** were found to crystallise in the triclinic $P\bar{1}$ space group, each containing six distinct U sites (U1–U5 in full occupancy and U6 modelled in half occupancies as it is on a centre of symmetry, Tables S3 and S4, ESI†) in the asymmetric unit. Two of these sites exist in an octahedral geometry (U1 and U6) and four in a pentagonal bipyramidal coordination geometry (U2–U5). In both structures, the Er/Y^{3+} species exists in an 8-coordinate, trigonal prismatic geometry, with both materials found to be isostructural.

Table 2 Crystal data and structure refinement details for compounds **UOF-Er** and **UOF-Y**

Compound	**UOF-Er**	**UOF-Y**
CSD	2192944	2192943
Empirical formula	$ErO_{22.5}U_{5.5}$	$YO_{22.5}U_{5.5}$
Formula weight	1836.43	1758.08
Crystal system	Triclinic	Triclinic
Space group	$P\bar{1}$	$P\bar{1}$
a (Å)	8.1060(16)	8.0890(16)
b (Å)	11.435(2)	11.408(2)
c (Å)	11.582(2)	11.517(2)
α/(°)	111.33(3)	111.13(3)
β/(°)	102.97(3)	103.02(3)
γ/(°)	106.48(3)	106.40(3)
Volume (Å^3)	892.0(4)	885.2(4)
Z/μ (mm^{-1})	2/54.500	2/53.474
Min./Max. θ [°]	2.030/24.999	2.037/24.999
d_{calcd} (g cm^{-3})	6.837	6.596
GOF	1.070	1.123
Final R_1 [a][$I > 2\sigma(I)$]	0.0914	0.0468
Final wR_2 [b][$I > 2\sigma(I)$]	0.2623	0.1402

[a] $R_1 = \sum||F_o|-|F_c||/|F_o|$. [b] $wR_2 = \{\sum[w(F_o^2 - F_c^2)^2]/\sum[w(F_o^2)^2]\}^{1/2}$.

Examination of the broader structure of **UOF-Er** and **UOF-Y** reveals that the material exists as a framework-type structure, with the secondary cations (Er^{3+}/Y^{3+}) lying within the channels of the framework (Fig. 2a). The backbone of the framework is composed of two distinct structural features. The first of these

are uranyl polyhedra sheets connected through O–O equatorial edges of U3–U6 to form β-U_3O_8-type layers (Fig. 2b). These polyhedra sheets consist of two distinct chains of the pentagonal bipyramidal U3–U5 in a –(U3-U5-U4-U4-U5-U3)– motif, with these chains linked by U1 and U6 octahedra. A pair of U2 centers are connected by edge-shared O–O, which pillar the β-U_3O_8-type layers through U1, U3 and U4 (Fig. 2c). The axial oxygens of U4–U6 coordinate the 8-coordinate Er/Y, which are also coordinated to four water molecules and located in the channels of the framework (Fig. 2d and e).

The octahedral U1 consists of two axial U=O bonds ranging from 1.821(14) to 1.939(14) Å, and four equatorial U–O bonds of 2.15(3) to 2.234(13) Å. These bond lengths, along with the near linear bond angle (176.0(15)°–176.5(6)°) of the two axial U=O bonds, are consistent with similar octahedral uranyl units reported for other UOH/F materials in the literature.[10,22,44,45] The four U sites existing in a pentagonal bipyramidal geometry (U2–U5), have two axial U=O bonds of 1.72(3) to 2.001(13) Å and O=U=O angles of 173.3(6)° to 178.8(6)°, and five equatorial U–O bonds of 2.210(13) to 2.53(3) Å. As with the U1 site, these values are broadly consistent with those previously reported.[10,22,44,45] The U6 site contains four O atoms at shorter U–O distances of 2.05(3) to 2.08(4) Å, arranged in a distorted square, and two axial oxygen atoms with slightly longer U–O bonds of 2.14(4) Å, which coordinate to the secondary metal cations.

From the BVS calculations (Tables S3 and S4, ESI†), assuming the presence of U^{6+} (R_{U-O} = 2.051; B = 0.519),[9] it can be determined that five of the six U centers (U1–U5) in both **UOF-Er** and **UOF-Y** exist as U^{6+}, as expected. Interestingly, the U6 site in both materials, having calculated BVS values of 5.58 and 5.54, suggests the presence of U^{5+} at this site in the structure. This is consistent with previously reported UOF structures, wherein U^{5+} sites have been observed at the octahedral U site which coordinates the secondary cations.[21,22] The oxygen donors were found to be a majority O, with four H_2O molecules coordinated to the Er/Y cations, a coordinated OH (O17 disordered in two positions) linking two U5 centers, and two more OH groups for O3 and O19. Based on the unit cell content and the types of U and O, the general formula is simplified to Z = 1: $M_2(H_2O)_8[(UO_2)_{10}UO_{14}(OH)_3]$, where M = Er for **UOF-Er** and Y for **UOF-Y**. As such, the structure complexity for the UOFs, measured by I_{chem} (bits/formula),[11] is ~114.5, quite complex given the average structure complexity of all known UOH minerals is ~76.

Of significant interest is the identified $P\bar{1}$ space group. Whilst layered UOH structures have been reported in the same space group,[30,45] no triclinic UOF has been identified yet in the literature. Looking along the channels of the framework (Fig. 2e), it is immediately apparent that the $(Er/Y)^{3+}$ ions don't lie in the center of the channel, instead lying closer to a corner of the space, with each Er/Y ion not connected to the next Er/Y ions lying in the channel. This is distinctly different from previously reported UOF structures, which are highlighted in Table 3. In these earlier structures, the interlayer cations form –(M–O–M)– chains along the channels, with these chains composed of two or more unique cation species.[21,22] In these sequences, the interlayer cations are separated by distances of ~3.8–4.0 Å, however for **UOF-Er** and **UOF-Y** this interaction distance is 5.8–6.2 Å, possibly explaining the lack of connectivity between the cations. Also, of interest is that in these previously reported materials, these cation species are disordered, existing across two sites in partial occupancies, allowing them to be aligned well inside the framework channels. However, in

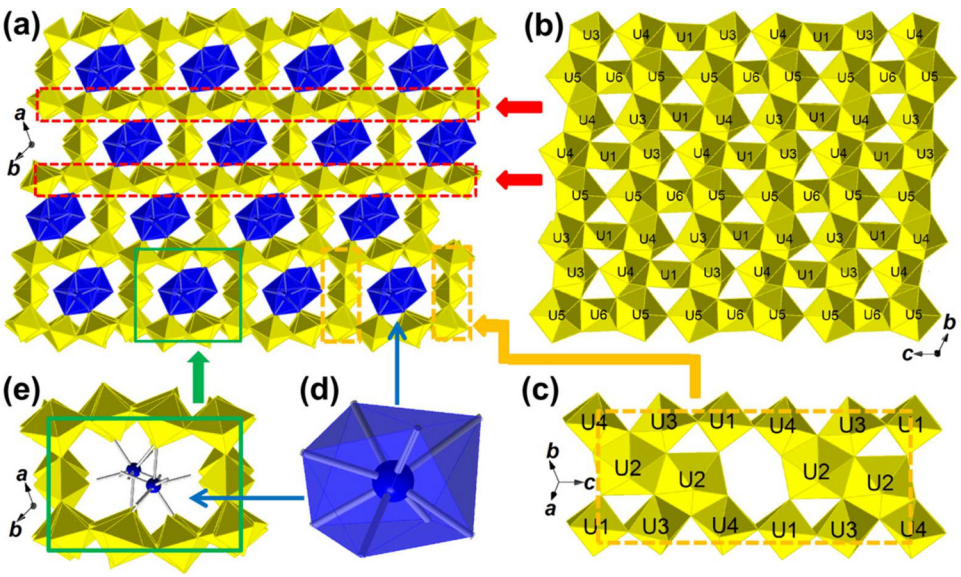

Fig. 2 Crystal structure of compound **UOF-Er/UOF-Y**: a polyhedral crystal structure along the *c*-axis (a), a polyhedral view of a uranyl oxide hydroxide layer with a β-U_3O_8 topology (b), the uranyl oxide hydroxide layers linked by double U2 pentagonal bipyramids (c), with 8-fold coordinated Er/Y (III) interlayer cations in the framework channels [(d) and (e)], U in yellow and Er/Y in blue.

Table 3 A summary of all available UOF-Ln/Y compounds

Compound	Space group, formula and cell parameters	Asymmetric unit[a]	Ln/Y ions	Topology
UOF-Eu/Gd[22]	$C222_1$: orthorhombic $(Eu/Gd)_2(OH)(H_2O)_5[(UO_2)_{10}O_{10}(OH)_2][(UO_4)(H_2O)_2]$ a = 11.629(2), b = 20.973(4), c = 14.170(3) Å	4 U (1), 3 U (0.5), Eu/Gd (0.65, 0.35)	Eu/Gd disordered on 2 sites	3^9,5,6^3,7^4,8-c net
UOF-Sm[21]	$C2$: monoclinic $Sm_2(OH)(H_2O)_5[(UO_2)_{10}O_{10}(OH)_2][(UO_4)(H_2O)_2]$ a = 11.626(2), b = 20.975(4), c = 14.199(3) Å; β = 90.04(3)°	11 U (1), 2 Sm (0.65, 0.35)	Sm disordered on 2 sites	3^18,5^3,6^4,7^6,8^2-c net
UOF-Er/Y	$P\bar{1}$: triclinic $(Er/Y)_2(H_2O)_8[(UO_2)_{10}UO_{14}(OH)_3]$ a = 8.1060(16), b = 11.435(2), c = 11.582(2) Å; α = 111.33(3)°, β = 102.97(3)°, γ = 106.48(3)°	5 U (1), 1 U (1/2), Er/Y (1)	Er/Y on 1 site	3^8,4,5^2,6^2,7^2-c net

[a] Site occupancy in brackets.

UOF-Er and **UOF-Y** these cation species have full occupancy preventing them alignment in the center of the channels. A second distinct, but related, difference is the chemical environment about the U1 and U3 centers. Each of these U centers contains axial O atoms projecting into the channel of the framework (O3 and O9, respectively) with relatively longer U═O bonds leading to lower-than-normal BVS values for O3 and O9. Whereas in previously reported structures[21,22] these oxygen species are involved in the coordination of the interlayer cation species, oxygens in the two new structures remain unbound, resulting in a unique pore environment yet unseen in UOF structures. This is further confirmed by the calculated crystal topologies (Table 3) for each of the UOF systems which show that the UOF-Er/Y system is distinct from those previously reported.

3.3. TEM characterization

Given their isostructural nature, only **UOF-Er** was further studied with TEM. A high-resolution TEM (HRTEM) image (Fig. 3) shows crystal lattice fringes. In Fig. 3, variations in the crystal fragment thickness, plus the presence of nano-domains highlight a complex structure. The selected area electron diffraction (SAED) pattern (inset in Fig. 3), viewed down the [3 5 9] zone axis, is indexed to the $P\bar{1}$ space group. In addition, electron diffraction spots correlating to a 3× superstructure along the [1 −6 3] direction, marked with arrows, are also evident, indicating the presence of a modulated structure. The extra Bragg maxima fall around the 5.8 Å region, in real space, and also show splitting.

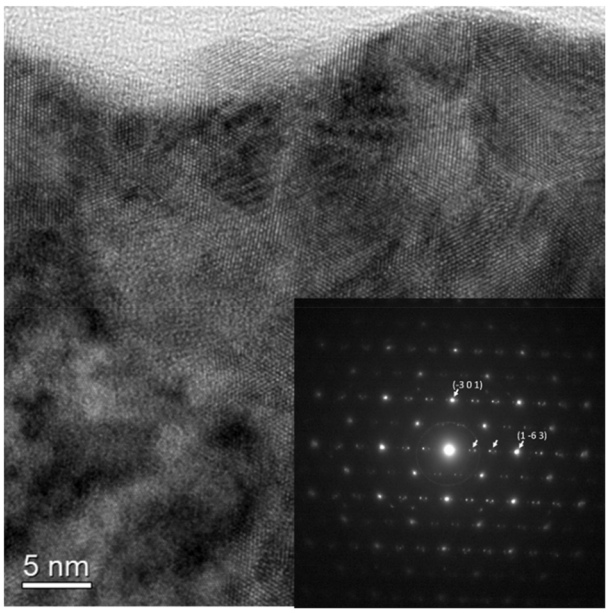

Fig. 3 HRTEM of **UOF-Er**: a high-resolution TEM image with an inset of a selected area electron diffraction pattern viewed down the [3 5 9] zone axis, also highlighting Bragg maxima from a modulated structure (arrows) along the (1 −6 3) direction indicating a 3× superstructure.

3.4. Electronic structures and uranium valences

To further investigate the potential for U^{5+} being present in both **UOF-Er** and **UOF-Y**, the U valences were characterised using DRS. This technique has been employed in the past to analyse U valences in UOH/F materials,[20,24] as it allows for the distinction between U^{4+}, U^{5+} and U^{6+}. The U^{4+}, having a $5f^2$ electronic configuration, gives both sharp (zero-phonon lines) and broad (vibronic) absorptions across both the infrared and visible spectrum ranges.[46] The presence of U^{5+} ($5f^1$) is categorised by peaks limited to the near infrared. These peaks are due to the crystal-field splitting of $^2F_{5/2}$–$^2F_{7/2}$, giving rise to distinct transitions in the range of 1538–833 nm (6500–12 000 cm^{-1}).[46,47] Lastly U^{6+} ($5f^0$), having no f electrons, has only charge-transfer bands which are visible in the UV and far UV regions of the spectrum.

The first feature of note in the spectra for both **UOF-Er** and **UOF-Y** (Fig. 4) is the broad, indistinct absorption between 250–550 nm. The two absorption maxima present in **UOF-Y** (Fig. 4a, top) at 350 nm and 450 nm can be attributed to the charge transfer of U^{6+}, which is consistent with values found for other uranyl oxide compounds.[48,49] The same feature is less visible in the **UOF-Er** spectrum, however given the location and broadness, is also attributed to U^{6+} charge transfer. Also located in this region, and possibly contributing to the broadness of the peak, are Er^{3+} f–f transitions (Fig. S4, ESI†). Examination of the NIR region (Fig. 4b) shows distinct peaks, strongly suggesting the presence of U^{5+} in both materials. For **UOF-Er** (Fig. 4b, bottom), this is signified by the strong, sharp peak at 910 nm/1490 nm. Two other peaks are also evident in

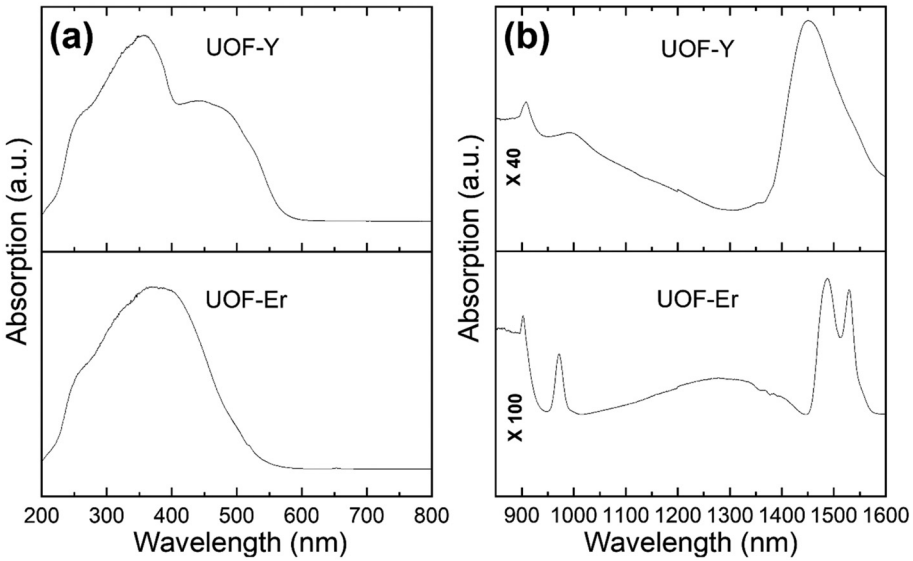

Fig. 4 The DRS spectra of **UOF-Er** and **UOF-Y** in the (a) UV-vis and (b) the near infrared regions.

this spectrum, which can be attributed to the Er^{3+} $^4I_{15/2} \rightarrow {}^4I_{11/2}$ (970 nm) and $^4I_{15/2} \rightarrow {}^4I_{13/2}$ (1556 nm) transitions.[50] The first thing of note in the NIR spectrum for **UOF-Y** (Fig. 4b, top) is the absence of the peaks at 970 and 1556 nm, further evidence towards their assignment as Er^{3+} transitions. Importantly however is that the same peak attributed to U^{5+}, whilst obfuscated, is evident in the spectrum of **UOF-Y** at 910 nm. Thus, the evidence of this peak, along with the BVS and crystal data, strongly suggests both **UOF-Er** and **UOF-Y** are mixed uranium valence compounds.

3.5. Vibrational modes

The vibrational modes of both materials were examined using Raman spectroscopy, which is shown in Fig. 5. Previous studies on such UOH and UOF materials have identified the regions relating to $\nu_2(\delta)(UO_2)^{2+}$ between 200–300 cm^{-1} with broad, weak peaks, $\nu(U_3O)$ and $\gamma[U_3(OH)_3]$ in the range of 300 to 600 cm^{-1} as broad, medium peaks and $\nu_1(UO_2)^{2+}$ between 700 and 900 cm^{-1} with sharp, strong peaks.[49,51] In exploring the spectrum for **UOF-Er** (Fig. 5a), a sharp, strong peak is evident at ~840 cm^{-1}, corresponding to the U═O bonds. The broader peaks between 150–550 cm^{-1} can be assigned to the various U–O bonds within the material. Despite a poorly resolved spectrum for **UOF-Y** (Fig. 5b), these same peaks are also visible, an expected result given the two materials are isostructural. Note the absence of Raman vibrations for the $(UO_2)^+$ uranyl ion is consistent with the crystallographic results that U^{5+} ions in these compounds are present in an octahedral coordination environment, similar to the U^{5+} ions in $Y_{0.51}U_{0.49}Ti_2O_6$ or $Eu_{0.53}U_{0.47}Ti_2O_6$ brannerite.[52]

3.6. Implications and perspectives

The herein reported synthesis of two isostructural, novel UOF structures clearly demonstrates that the scope of lanthanides

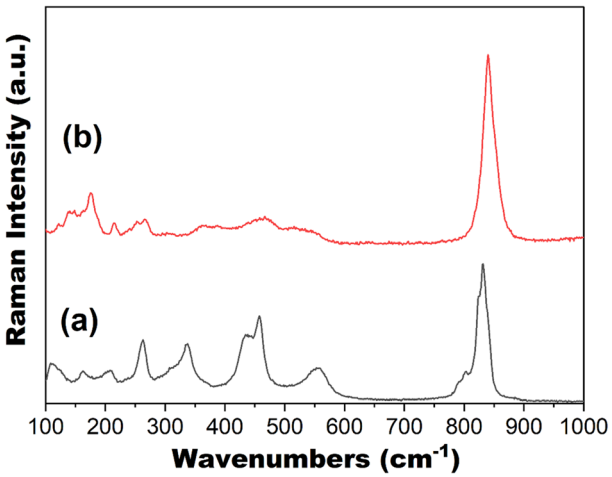

Fig. 5 The Raman spectra of **UOF-Er** (a) and **UOF-Y** (b).

which can be introduced into these framework-type structures is much broader than previously hypothesised with Er^{3+}, Sm^{3+}, Eu^{3+} and Gd^{3+}, also including Y^{3+}, now all reported in synthetic UOF materials. The structural parameters also appear to fit well to that of wyartite, the first pentavalent-uranium mineral.[53,54] The use of higher solution pH and different hydrothermal conditions in this study compared to that previously reported is also of interest. The solution pH is one of the driving forces leading to the final products. While the initial hydrolysed uranyl species, $[(UO_2)(OH)]^+$, is less than 5% at the solution pH < 4, it increases to nearly 15% at the solution pH ~ 4.5.[55] Further hydrolysed uranyl species such as $[(UO_2)(OH)_2]$, $[(UO_2)_2(OH)_2]^{2+}$ and $[(UO_2)_3(OH)_5]^+$ will be present at the solution pH above 5. These findings clearly suggest that the flexible β-U_3O_8 type layer which makes up the backbone of the framework tolerates subtle structural changes,

which in turn allows for a variety of conditions and secondary metal ions to be used in their synthesis. This highlights that more work is required in this area to gain a better understanding of the diversity tolerated by these materials whilst maintaining UOF formation.

However, given the hydrothermal conditions used in this study could sensibly be comparable to the conditions found in the geological repositories used for storing SNF, the understanding garnered from the synthesis **UOF-Er** and **UOF-Y** can be extended to better understanding the alteration chemistry of UO_2 based species in these SNF environments. As the results in this study are examining the high temperature chemistry of these materials over a short time period (days), this work best captures the early stages of the alteration chemistry in these repositories. Further time under these high temperature conditions could exacerbate these changes, or even lead to further changes within these materials, and thus warrants further study.

The implication of the reported UOFs may extend to broader work on nuclear materials as well. Work has previously been performed on incorporating lanthanides as surrogates of minor actinides (*i.e.* Ce^{4+}/Nd^{3+} in place of Pu^{4+}/Cm^{3+}) as the interlayer cations of UOH-based minerals.[25,26] Given the ionic radii of 8-coordinate Er^{3+} ($R_{CN\,=\,8}$ = 1.004 Å) and Y^{3+} ($R_{CN\,=\,8}$ = 1.019 Å) closely match that of Cm^{3+} ($R_{CN\,=\,8}$ = 0.97 Å),[56] it stands to reason that the incorporation of this cation into a similar UOF structure as the one reported here may be possible.

A recent study by Murphy and co-workers examined the intercalation of the anionic IO_3^- species within a UOH structure,[57] which is the first such study incorporating an anionic species into these materials. The authors proposed that in capturing the radiolytic IO_3^- this slowed its release into the biosphere, and thus the presence of the UOH material in a geological repository could prove beneficial. It stands to reason that this work could be extended to other anions present in SNF such as pertechnetate $(TcO_4)^-$, with the framework-type structure of UOFs possibly offering additional benefits.

4. Conclusions

Two new UOFs with incorporated Er^{3+}/Y^{3+} ions have been synthesised under hydrothermal conditions using uranyl nitrate as the U precursor. The U/(Er/Y) ratio of 5.5 matches those found for previously reported UOFs with other lanthanide ions, however the triclinic $P\bar{1}$ space group is novel amongst previously reported framework-type structures. The pentagonal bipyramidal and octahedral uranium polyhedra extend to form β-U_3O_8-type sheets, which are pillared by an additional pentagonal bipyramidal uranium center to form the backbone of the framework, with the secondary Er^{3+}/Y^{3+} cations found within the channels. Unlike previously reported UOFs, the secondary cations are not interconnected, instead existing as a single cation species. The presence of U^{5+} in the structure was confirmed by DRS, existing as pentavalent uranium at one of the octahedral coordination sites.

These compounds, in expanding the knowledge previously obtained from published UOF structures, clearly demonstrate the complex, flexible and highly sensitive chemistry which governs the formation and reactivity of uranium oxide hydrate-based systems which is dependent on, amongst other things, temperature, redox potential, and pH. Further work is still warranted to develop this understanding, with systematic laboratory studies controlling and exploring these conditions on such way to extra thus knowledge.

Author contributions

T. A. Ablott: Conceptualization, data curation, formal analysis, writing – original draft, writing – review & editing. K. T. Lu: Data curation, formal analysis, writing – review & editing. R. D. Aughterson: Data curation, formal analysis, writing – review & editing. Y. Zhang: Conceptualization, data curation, formal analysis, project administration, resources, supervision, writing – original draft, writing – review & editing.

Conflicts of interest

There is no conflict of interest.

Acknowledgements

We would like to thank I. Karatchevtseva for Raman measurement, the Nuclear Science and Technology (NST) at ANSTO for synthesis and characterization of materials. The crystallographic data for compounds **UOF-Er** and **UOF-Y** were collected on the MX2 beamline at the Australian Synchrotron, a part of ANSTO, and made use of the Australian Cancer Research Foundation (ACRF) detector.

References

1 J. Plásil, *J. Geosci.*, 2014, **59**, 99–114.
2 R. J. Baker, *Coord. Chem. Rev.*, 2014, **266–267**, 123–136.
3 Y. Zhang, T. Wei, A. Xu, P. Dayal and D. J. Gregg, *J. Am. Ceram. Soc.*, 2021, **104**, 5981–5989.
4 S. Alyokhina, *Nucl. Eng. Technol.*, 2018, **50**, 717–723.
5 J. Janeczek and R. C. Ewing, *J. Nucl. Mater.*, 1992, **190**, 157–173.
6 J. Janeczek and R. C. Ewing, *J. Nucl. Mater.*, 1992, **190**, 128–132.
7 R. J. Finch and R. C. Ewing, *J. Nucl. Mater.*, 1992, **190**, 133–156.
8 D. J. Wronkiewicz, J. K. Bates, S. F. Wolf and E. C. Buck, *J. Nucl. Mater.*, 1996, **238**, 78–95.
9 P. C. Burns, R. C. Ewing and F. C. Hawthorne, *Can. Mineral.*, 1997, **35**, 1551–1570.

10 P. C. Burns, in *Structural Chemistry of Inorganic Actinide Compounds*, ed. S. V. Krivovichev, P. C. Burns and I. G. Tananaev, Elsevier, Amsterdam, 2007, pp. 1–30.
11 J. Plásil, *Eur. J. Mineral.*, 2018, **30**, 237–251.
12 Y. Zhang, K. T. Lu and R. Zheng, *Dalton Trans.*, 2022, **51**, 2158–2169.
13 N. G. Chernorukov, O. V. Nipruk, G. N. Chernorukov, R. V. Abrazheev and K. A. Chaplieva, *Russ. J. Gen. Chem.*, 2019, **89**, 71–75.
14 R. Vochten, L. van Haverbeke and R. Sobry, *J. Mater. Chem.*, 1991, **1**, 637–642.
15 Y. Li and P. C. Burns, *Can. Mineral.*, 2000, **38**, 737–749.
16 R. E. Glatz, Y. Li, K.-A. Hughes, C. L. Cahill and P. C. Burns, *Can. Mineral.*, 2002, **40**, 217–224.
17 P. C. Burns and F. C. Hill, *Can. Mineral.*, 2000, **38**, 163–173.
18 Y. Zhang, J. Čejka, G. R. Lumpkin, T. T. Tran, I. Aharonovich, I. Karatchevtseva, J. R. Price, N. Scales and K. Lu, *New J. Chem*, 2016, **40**, 5357.
19 K. A. Kubatko and P. C. Burns, *Inorg. Chem.*, 2006, **45**, 10277–10281.
20 K. T. Lu, Y. Zhang, T. Wei, T. A. Ablott, T. H. Nguyen and R. Zheng, *New J. Chem*, 2022, **46**, 1371.
21 K. T. Lu, Y. Zhang, T. Wei, Z. Wang, D. T. Oldfield and R. Zheng, *Inorg. Chem.*, 2021, **60**, 13233–13241.
22 K. T. Lu, Y. Zhang, R. D. Aughterson and R. Zheng, *Dalton Trans.*, 2020, **49**, 15854–15863.
23 Y. Li and P. C. Burns, *Can. Mineral.*, 2000, **38**, 1433–1441.
24 Y. Zhang, T. Wei, T. T. Tran, K. T. Lu, Z. Zhang, J. R. Price, I. Aharonovich and R. Zheng, *Inorg. Chem.*, 2020, **59**, 12166–12175.
25 C. W. Kim, D. J. Wronkiewicz, R. J. Finch and E. C. Buck, *J. Nucl. Mater.*, 2006, **353**, 147–157.
26 S. Biswas, R. Steudtner, M. Schmidt, C. McKenna, L. L. Vintró, B. Twamley and R. J. Baker, *Dalton Trans.*, 2016, **45**, 6383–6393.
27 Y. Zhang, R. Aughterson, I. Karatchevtseva, L. Kong, T. T. Tran, J. Čejka, I. Aharonovich and G. R. Lumpkin, *New J. Chem.*, 2018, **42**, 12386–12393.
28 K. T. Lu, Y. Zhang, T. Wei, J. Čejka and R. Zheng, *Dalton Trans.*, 2020, **49**, 5832–5841.
29 Y. Zhang, R. D. Aughterson, Z. Zhang, T. Wei, K. Lu, J. Čejka and I. Karatchevtseva, *Inorg. Chem.*, 2019, **58**, 10812–10821.
30 L. N. G. Chernorukov, O. V. Nipruk, K. A. Klin, G. N. Chernorukov and O. N. Tumaeva, *Radiochemistry*, 2021, **63**, 110–120.
31 D. Aragão, J. Aishima, H. Cherukuvada, R. Clarken, M. Clift, N. P. Cowieson, D. J. Ericsson, C. L. Gee, S. Macedo, N. Mudie, S. Panjikar, J. R. Price, A. Riboldi-Tunnicliffe, R. Rostan, R. Williamson and T. T. Caradoc-Davies, *J. Synchrotron Radiat.*, 2018, **25**, 885–891.
32 W. Kabsch, *Acta Crystallogr., Sect. D: Biol. Crystallogr.*, 2010, **66**, 133–144.
33 G. M. Sheldrick, *SADABS, Empirical Absorption and Correction Software*, University of Göttingen, Göttingen, Germany, 1996.
34 G. M. Sheldrick, *Acta Crystallogr., Sect. A: Found. Adv.*, 2015, **71**, 3–8.
35 G. M. Sheldrick, *Acta Crystallogr., Sect. C: Struct. Chem.*, 2015, **71**, 3–8.
36 O. V. Dolomanov, L. J. Bourhis, R. J. Gildea, J. A. K. Howard and H. Puschmann, *J. Appl. Crystallogr.*, 2009, **42**, 339–341.
37 V. A. Blatov, A. P. Shevchenko and D. M. Proserpio, *Cryst. Growth Des.*, 2014, **14**, 3576–3586.
38 M. O'Keeffe, M. A. Peskov, S. J. Ramsden and O. M. Yaghi, *Acc. Chem. Res.*, 2008, **41**, 1782–1789.
39 E. V. Alexandrov, V. A. Blatov, A. V. Kochetkov and D. M. Proserpio, *CrystEngComm*, 2011, **13**, 3947–3958.
40 V. A. Blatov and A. P. Shevchenko, *Struct. Chem.*, 2021, **32**, 507–519.
41 E. V. Alexandrov, A. P. Shevchenko and V. A. Blatov, *Cryst. Growth Des.*, 2019, **19**, 2604–2614.
42 M. K. Pagoaga, D. E. Appleman and J. M. Stewart, *Am. Mineral.*, 1987, **72**, 1230–1238.
43 F. Zocchi, *J. Mol. Struct.: THEOCHEM*, 2007, **805**, 73–78.
44 P. C. Burns, *Can. Mineral.*, 2005, **43**, 1839–1894.
45 M. Rivenet, N. Vigier, P. Roussel and F. Abraham, *J. Solid State Chem.*, 2009, **182**, 905–912.
46 K. S. Finnie, Z. Zhang, E. R. Vance and M. L. Carter, *J. Nucl. Mater.*, 2003, **317**, 46–53.
47 Y. Zhang, T. Wei, Z. Zhang, L. Kong, P. Dayal and D. J. Gregg, *J. Am. Ceram. Soc.*, 2019, **102**, 7699–7709.
48 Y. Zhang, J. K. Clegg, K. Lu, G. R. Lumpkin, T. T. Tran, I. Aharonovich, N. Scales and F. Li, *ChemistrySelect*, 2016, **1**, 7–12.
49 Y. Zhang, M. Bhadbhade, I. Karatchevtseva, J. R. Price, H. Liu, Z. Zhang, L. Kong, J. Čejka, K. Lu and G. R. Lumpkin, *J. Solid State Chem.*, 2015, **226**, 42–49.
50 W. T. Carnall, P. R. Fields and K. Rajnak, *J. Chem. Phys.*, 1968, **49**, 4424.
51 R. L. Frost, J. Čejka and M. L. Weier, *J. Raman Spectrosc.*, 2007, **38**, 460–466.
52 Y. Zhang, I. Karatchevtseva, L. Kong, T. Wei and Z. Zhang, *J. Am. Ceram. Soc.*, 2018, **101**, 5219–5228.
53 F. C. Hawthorne, R. J. Finch and R. C. Ewing, *Can. Mineral.*, 2006, **44**, 1379–1385.
54 P. C. Burns and R. J. Finch, *Am. Mineral.*, 1999, **84**, 1456–1460.
55 C. Moulin and P. Decambox, *Anal. Chem.*, 1995, **67**, 348–353.
56 R. D. Shannon, *Acta Crystallogr., Sect. A: Cryst. Phys., Diffr., Theor. Gen. Crystallogr.*, 1976, **32**, 751–767.
57 G. L. Murphy, P. Kegler, M. Klinkenberg, A. Wilden, M. Henkes, D. Schneider and E. V. Alekseev, *Dalton Trans.*, 2021, **50**, 17257–17264.